Original article

Applicability of the MIKE21 Model for Simulating the Rip Current: A Case Study for Cam Ranh Bay, Khanh Hoa Coastal of Vietnam

N. T. Ngo [1, 2], T. B. Nguyen [3, 4] ✉

[1] *Ho Chi Minh City University of Natural Resources and Environment, Ho Chi Minh City, Vietnam*
[2] *VNU University of Science, Ho Chi Minh City, Vietnam*
[3] *Ho Chi Minh City University of Technology, Ho Chi Minh City, Vietnam*
[4] *Vietnam National University, Ho Chi Minh City, Vietnam*
✉ *ntbay@hcmut.edu.vn*

Abstract

Purpose. Numerous drownings have been recorded killing dozens of beach bathers along the coastal zones of Khanh Hoa Province in Vietnam, most of which are recognized to be related to rip currents in recent years. The object of the study was, therefore, to simulate the rip current generations (RCGs) along the Bai Dai Beach of Cam Ranh Bay in Khanh Hoa Province, Vietnam by applying the MIKE21-NSW Model.

Methods and Results. In order to deploy this study, field surveys were conducted to collect the hydrodynamic characteristics and seabed topography during the period from December 10, 2012, to January 20, 2013. The performance of the MIKE21-NSW Model has been appraised by comparing the simulated results with the observed data and was in good agreement with SEIs (NASH = = 0.76÷0.94, RMSE = 2.1÷14.1% and R^2 = 0.79÷0.95).

Conclusions. Based on comparing the simulated model with the observed data, it was stated that the MIKE21-NSW Model can effectively characterize the rip current hazard for different beach surface states. The findings provide a useful reference for beach development management and early warm rip current across the study beach.

Keywords: MIKE21-NSW Model, rip current, seaward current, surf zone, wave-current interaction

Introduction

The rip current recorded on many beaches around the world is considered a potential hazard to beach bathers [1, 2]. It is known as a high-speed seaward current that flows in a narrow bottom channel from the surf break zone of the wave [3, 4]. The propagation of waves towards the shore is affected by the topographic, causing uneven breaking and subsequent formation of rip currents driven by radiation stress [5, 6]. As the wave size keeps increasing, the amount of water pushed toward the shore also increases, resulting in the break waves that push toward the shore [1, 7]. When the waves no longer approach the shore, a high-water accumulation due to

the break waves toward the shore cannot move longshore, and seaward currents with high speed are formed, which are called rip currents [8, 9].

The rip current is rated as one of the main drowning factors in coastal beach baths, annually leading to hundreds of deaths worldwide [1, 10]. The recorded drowning events, which are closely related with rip currents, are increasing every year [11, 12]; hence, understanding the RCGs will contribute to predicting the beach state as well as issuing early warnings to beachgoers [13, 14]. Almost issued studies have indicated that the RCGs are closely related to hydrodynamic factors such as waves, currents, tides, and seabed topography structure, as well as weather factors such as wind, tropical depression, and typhoons [15, 16].

Nowadays, there are varieties of methodologies to track as well as predict the rip current, including field observations [8, 10, 17, 18], laboratory experiments [6, 19], camera and Global Positioning System (GPS) system [11, 18], as well as numerical model simulation [10, 17, 18]. For example, there was a study on the RCGs from a macrotidal beach in the southwestern U.K. based on over 87 tidal cycle databases, which stated that the RCGs are very sensitive over a range of temporal and spatial scales of the tides [7].

Being recognized as one of the most famous beaches in Vietnam, the Bai Dai Beach has welcomed an increase in domestic and foreign tourists in recent years [20, 21]. However, drowning events due to rip currents have been increasingly recorded there [21]. Underlying public concern about the unsafety of the Bai Dai Beach as well as other baths, several studies on the RCGs have been implemented to address the potential risks [21]. However, the studies on the RCGs have not been implemented comprehensively for the Bai Dai Beach of Cam Ranh Bay. The study is, therefore, deployed to evaluate the RCGs across the Bai Dai Beach for the purpose of supporting the management of bathing activities as well as providing an early warning about the potential risks caused by rip currents.

Materials and methods of research

Study area. The Bai Dai Beach bath is located in the center of Nha Trang City, Khanh Hoa Province (Fig. 1). It is known as one of the most beautiful and famous beaches in Vietnam with a length of approximately 12 km [21].

It annually welcomes thousands of domestic and foreign tourists. The study area is dominated by tropical monsoon circulation with two main wind seasons namely the Northeast (November – March) and the Southwest (April – September) [21]. The study area recorded the appearance of rip currents following waves with great heights under the influence of the Northeast monsoon circulation [21, 22]. In recent years, the number of deaths by drowning related to rip currents has been increasingly recorded across the study beach [20, 21].
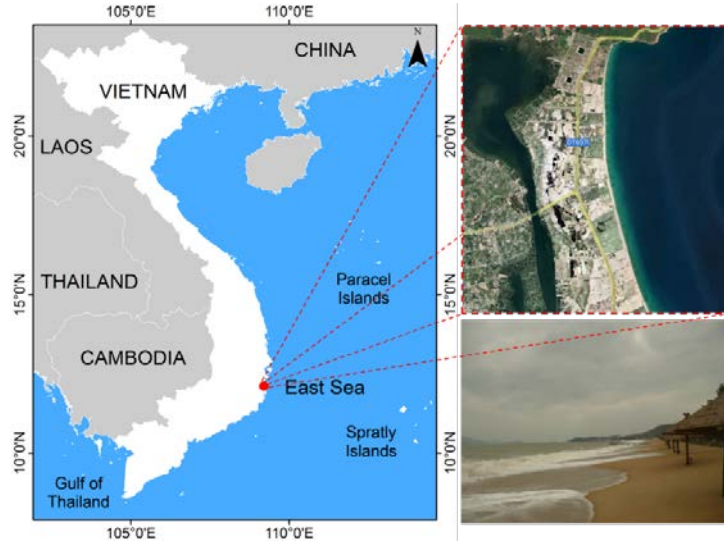
F i g. 1. Map of Vietnam presenting the location of the Bai Dai Beach

MIKE21-NSW description. MIKE21-NSW is an abbreviation for the nearshore spectral wind-wave module, developed by the Danish Hydraulic Institute (DHI) for simulating wave propagation involvement in nearshore areas [1]. It is known as one of the useful tools for simulating the effects of refraction and shoaling due to the change in nearshore bathymetry, local wind generation, and energy dissipation under the effect of seabed friction and wave breaking [10, 13, 21].

An advantage of applying the MIKE21-NSW Model is that the users can establish computational hydraulic grids based on mesh cage technique (e.g., quadrilateral mesh with large size nests, triangular mesh with small size nests) in simulating hydrodynamic problems and especially rip current simulation. An additional advantage of the MIKE21-NSW Model is that it was developed to be able to run the simulation of hydrodynamic and wave propagation problems on Graphics Processing Units (GPUs) of computer platforms, so the simulation running time of the MIKE21-NSW Model is less than the running time of other numerical models [1]. In addition, the module also considers the effect of wave-current interaction [17].

The MIKE21-NSW module operates based on the MIKE21-HD FM module [1]. The governing equations in the MIKE21-HD FM module are presented by equations

$$\frac{\partial h}{\partial t} + \frac{\partial h\bar{u}}{\partial x} + \frac{\partial h\bar{v}}{\partial y} = hS, \tag{1}$$

$$\frac{\partial h\bar{u}}{\partial t} + \frac{\partial h\bar{u}^2}{\partial x} + \frac{\partial h\overline{vu}}{\partial y} = f\bar{v}h - gh\frac{\partial \eta}{\partial x} - \frac{h}{\rho_0}\frac{\partial p_a}{\partial x} - \frac{gh^2}{2\rho_0}\frac{\partial \rho}{\partial x} + \frac{\tau_{sx}}{\rho_0} - \frac{\tau_{bx}}{\rho_0} -$$

$$-\frac{1}{\rho_0}\left(\frac{\partial s_{xx}}{\partial x} + \frac{\partial s_{xy}}{\partial y}\right) + \frac{\partial}{\partial x}(hT_{xx} + \frac{\partial}{\partial y}(hT_{xy}) + hu_sS, \tag{2}$$

---

[1] DHI, 2021. *MIKE 21 Spectral Waves FM: Spectral Wave Module. User Guide*. DHI A/S Publ., 122 p.

$$\frac{\partial h\bar{v}}{\partial t} + \frac{\partial h\overline{uv}}{\partial x} + \frac{\partial h\bar{v}^2}{\partial y} = -f\bar{u}h - gh\frac{\partial \eta}{\partial y} - \frac{h}{\rho_0}\frac{\partial p_a}{\partial y} - \frac{gh^2}{2\rho_0}\frac{\partial \rho}{\partial y} + \frac{\tau_{sy}}{\rho_0} - \frac{\tau_{by}}{\rho_0} -$$

$$-\frac{1}{\rho_0}\left(\frac{\partial s_{yx}}{\partial x} + \frac{\partial s_{yy}}{\partial y}\right) + \frac{\partial}{\partial x}\left(hT_{xy} + \frac{\partial}{\partial y}\left(hT_{yy}\right) + hv_sS, \right. \tag{3}$$

where t is the time, s; x and y are the coordinates in the Descartes coordinate system; η is the water level fluctuation, m; d is the water depth, m; h is the total water depth, m; g is the gravitational acceleration, m/s^2; $f = 2\,\Omega\sin$; ϕ is the Coriolis parameter; ρ_0 is the specific volume of water, kg/m^3; p_a is the atmospheric pressure, Pa/m; and u_s, v_s are the flow velocity components, m/s, in the x- and y-directions respectively; $\bar{u}$ and $\bar{v}$ are the depth-averaged velocity components, m/s, and they are defined by equation

$$\begin{cases} h\bar{u} = \int_{-d}^{\eta} u\,dz \\ h\bar{v} = \int_{-d}^{\eta} v\,dz. \end{cases} \tag{4}$$

The internal stress components (Tij) in equations (2) and (3) are determined by equation

$$\begin{cases} T_{xx} = 2A\frac{\partial \bar{u}}{\partial x} \\ T_{xy} = A\left(\frac{\partial \bar{u}}{\partial y} + \frac{\partial \bar{v}}{\partial x}\right) \\ T_{yy} = 2A\frac{\partial \bar{v}}{\partial y}. \end{cases} \tag{5}$$

In equation (5) A is the horizontal eddy viscosity coefficient, m^2/s; τ_{sx}, τ_{sy} are the surface friction stress in the x and y directions, respectively, N/m^2; τ_{bx}, τ_{by} are the bottom friction stress components in the x and y directions respectively, N/m^2; and S_{xx}, S_{xy}, and S_{yy} are the wave radiation stress (WRS) components in the x-y directions respectively, N/m^2.

To simulate WRS, the MIKE21-NSW Model uses wave balance equations for the Cartesian coordinate system [1] [23]. Specifically, the conservation equation of wave momentum is written in the Descartes coordinate system as follows:

$$\frac{\partial N}{\partial t} + \nabla(\vec{v}N) = \frac{S}{\sigma}, \tag{6}$$

where $N(\vec{x}, \sigma, \theta, t)$ is the influence density; σ is the relative angular frequency; θ is the wave direction; ∇ is the differential operator; and S is the root term of the energy balance equation.

In equation (6) S is defined by the equation

$$S = S_{nl} + S_{ds} + S_{bot.} + S_{surf.},$$ (7)

where S_{nl} is the wave energy created by the wind; S_{ds} is the energy dissipated by the white caps; S_{bot} is the wave energy due to bottom friction; and S_{surf} is the energy dissipated by the breaking wave. The propagation speed of wave group $\vec{V}(c_x, c_y, c_\sigma, c_\theta)$ in the four-dimensional space is defined by equation

$$S(c_x, c_y) = \frac{d\vec{x}}{dt} = \vec{c}_g + \vec{U},$$ (8)

where c_σ and c_θ are calculated by the following equations:

$$c_\sigma = \frac{d\sigma}{dt} = \frac{\partial\sigma}{\partial t}\left[\frac{\partial d}{\partial t} + \vec{U}\nabla_x d\right] - c_g \vec{k}\frac{\partial \vec{U}}{\partial s},$$ (9)

$$c_\theta = \frac{d\theta}{dt} = -\frac{1}{k}\left[\frac{\partial\sigma}{\partial d}\frac{\partial d}{\partial m} + \vec{k}\frac{\partial \vec{U}}{\partial m}\right].$$ (10)

In the MIKE21-NSW Model, the wave radiation stress components (S_{xx}, S_{xy}, and S_{yy}) are presented as surface forces representing the transport of kinetic energy through a surface, determined by the following equations:

$$S_{xx} = E\left(\left(\frac{kh}{\sinh 2kh} + \frac{1}{2}\right)\cos^2\theta + \frac{kh}{\sinh 2kh}\right),$$ (11)

$$S_{xy} = S_{yx} = E\left(\left(\frac{kh}{\sinh 2kh} + \frac{1}{2}\right)\sin\theta\cos\theta\right),$$ (12)

$$S_{yy} = E\left(\left(\frac{kh}{\sinh 2kh} + \frac{1}{2}\right)\sin^2\theta + \frac{kh}{\sinh 2kh}\right).$$ (13)

E is the wave energy and is defined by $E = 1/8\ \rho g H^2$; θ is the angle of the incident wave; H is the wave height; k is the number of waves; and h is the water depth at a defined position.

The relationship between angular frequency and wave number is defined by equation

$$\sigma^2 = gk\tanh kh,$$ (14)

σ in equation (14) is calculated by $\sigma = \frac{2\pi}{T} gk\tanh kh$.

Initial and boundary conditions. Firstly, the bathymetry data covering the study area for establishing the hydraulic grid were obtained from the Nha Trang Oceanography Institute (NTOI). The bathymetry data were collected in digital form of .xyz file format, corresponding to the longitude, latitude, and seabed depth. Next, these data were interpolated into each mesh point using the Kriging method based on Surfer 10 software (Fig. 2).
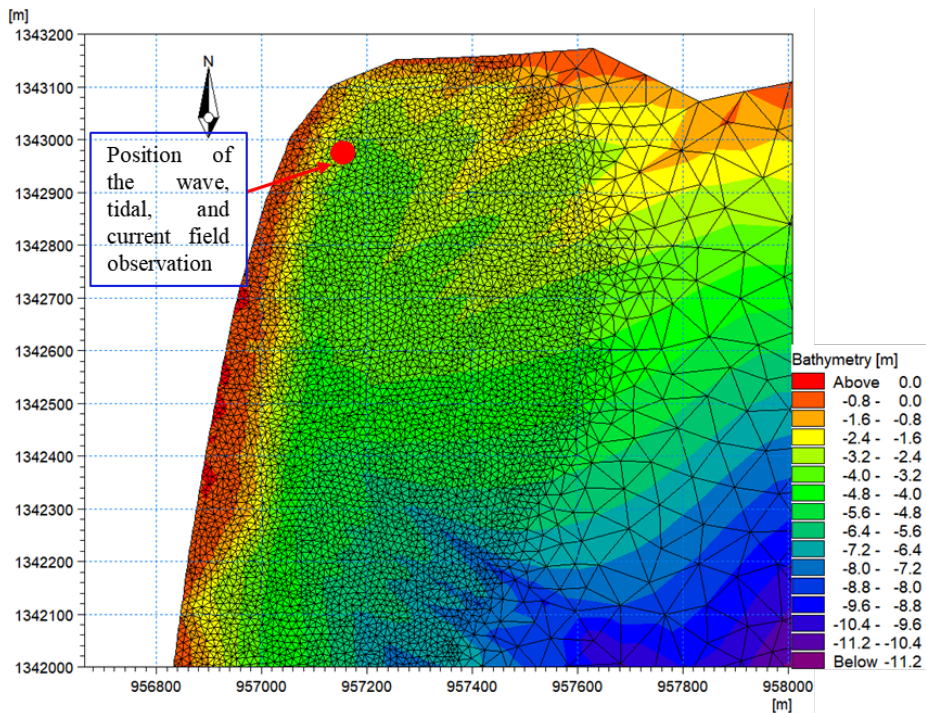
F i g. 2. Detailed hydraulic grid and position of the wave, tidal and current field observation across the study area

Finally, to save model simulation run time, an unstructured grid with change mesh space (sparse in the large seabed depth zones and thick in the study area where the seabed depth is shallow) is established, which is the best to reflect the conditions. In the simulation of the RCGs with irregular seabed geometry, water depth, sea surface state, and wind fields are always changing over time. Specifically, the water level data obtained from the NTOI, and the offshore boundary data (wave height, period, and frequency) obtained from the Global Reanalyzed Wave Data (GRWD) are applied as the input boundary data for the model simulation. In addition, other main hydrodynamic parameters are set up for simulating the MIKE21-NSW Model and are also presented in Table 1.

T a b l e 1

Hydrodynamic parameters for simulating the MIKE21-NSW Model

Parameters	Values	Notes
Δt	0.25 s	Time step
D_h	5.0 m²/s	Eddy viscosity coefficient
n	0.03125	Manning's coefficient
Vw	7–12 m/s	Wind speed
Hm	0.9–2.3 m	Wave height
Tm	4.3–7.0 s	Wave period
η	0 m	Initial water level fluctuations

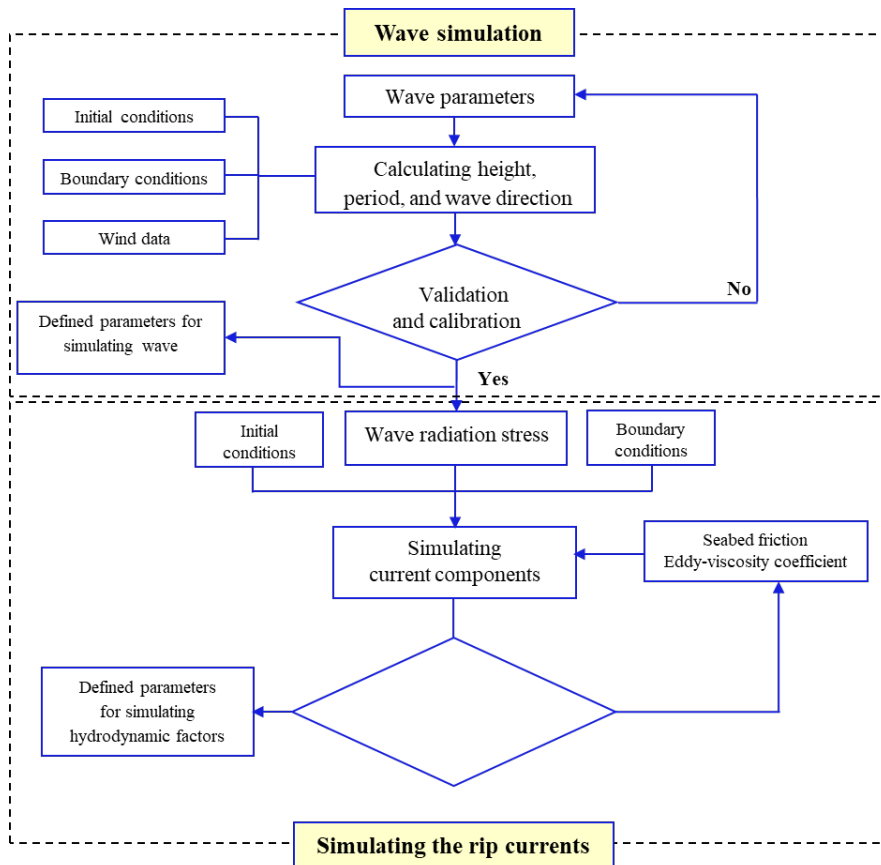The steps for implementing the rip current simulation are illustrated in Fig. 3.

F i g. 3. Flowchart for implementation steps of simulating the rip current

Research results and discussion

Model performance evaluation. The model performance was verified through validation and calibration procedures by comparing the simulated results of the hydrodynamic factors such as water level, wave height, and current field with the series of observed data. The agreement between the simulated results and the observed data of the hydrodynamic factors is valued based on the statistical error indices (SEIs) such as the Nash criterion (NASH), Root Mean Square Error (RMSE), and the goodness of fit (R^2). The above-mentioned SEIs are widely applied to quantitative performance of hydraulic models [8].

NASH index is defined by formula

$$\text{NASH} = \frac{\sum_{i=1}^{n}(U_O - \bar{U}_O)^2 - \sum_{i=1}^{n}(U_O - U_s)^2}{\sum_{i=1}^{N}(U_0 - \bar{U}_O)^2}. \tag{15}$$

The RMSE is calculated by formula

$$RMSE = \sqrt{\frac{1}{n}\sum_{i=1}^{n}(U_0 - U_s)^2}, \tag{16}$$

and the goodness of fit (R^2) is defined by formula

$$R^2 = 1 - \frac{\sum_{i=1}^{n}(U_s - U_0)^2}{\sum_{i=1}^{N}(U_s - \overline{U}_0)^2}, \tag{17}$$

where U_o and U_s are the observed data and the simulated result, respectively; n is the number of data points; and $\overline{U}_0$ is the mean value of the observed data series.

Specifically, the model validation was implemented in the period from 10 to 30 of December 2012, and the model calibration was performed in the period from 01 to 20 of January 2013. The model validation was conducted by comparing the simulated results of water level, wave height, and current field with the observed data during the period from 10 to 30 of December 2012 (Table 2). The results pointed out that the values of NASH, RMSE, and R^2 obtained comparing the simulated results of water level, wave height, and current field with the observed data varied from 0.76 ~ 0.89, 2.1 ~ 14.1%, and 0.79 ~ 0.91, respectively. In general, the validation results from Table 2 indicate that the selected hydrodynamic parameters (Table 1) for model simulation were stable and obtained the simulation results of hydrodynamic processes with high accuracy.

T a b l e 2

Performance of the MIKE21 Model through validation and calibration procedures

Type	Validation			Calibration		
	NASH	RMSE	R^2	NASH	RMSE	R^2
Water level	0.89	2.1%	0.91	0.94	9.1%	0.95
Wave height	0.76	14.1%	0.79	0.83	13.6%	0.84
Current field	0.79	2.7%	0.83	0.90	2.4%	0.91

Similarly, the model calibration was also deployed by comparing the simulated results of water level, wave height, and current field with the observed data during the period from 01 to 20 of January 2013. The results indicated that there was good agreement between the simulated results and the observed water levels (Fig. 4, *a*) through high values of NASH and R^2 (0.94 and 0.95, respectively) and a small error of RMSE (9.1%) (Table 2).

For the current field, a good fit between the simulated results and the observed data (Fig. 4, *b*) was also recorded with the SEIs (NASH = 0.90, RMSE = 2.4%, and R^2 = 0.91, respectively). High correlation values were also obtained by comparing the simulated results with the observed wave heights (Fig. 4, *c*) such as NASH = 0.83, RMSE = 13.6%, and R^2 = 0.84 respectively. According to [8],

the performance of hydrodynamic models is assessed satisfactorily if the values of SEIs equal NASH > 0.50, RMSE < 10%, and $R^2 \geq 0.70$. In general, the model performance through the calibration procedure had a good agreement between the simulated results and the observed data.
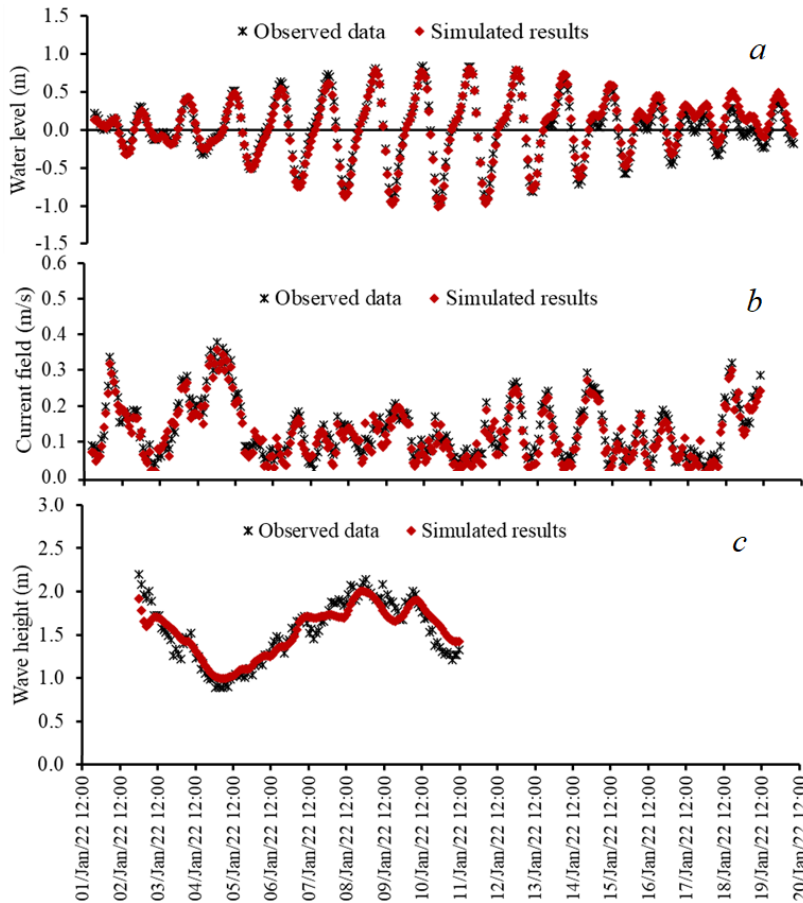
F i g. 4. Comparison of the simulated model and observed water level (*a*), current field (*b*) and wave height (*c*) at the extracted point (109°11'45.94"E; 12°6'46.43"N) with NASH, RMSE, and R^2 varying from 0.83 ~ 0.94, 2.4 ~ 13.6%, and 0.84 ~ 0.95

Simulation results of wave radiation stress. The simulated results of the WRS components across the study area are presented in Fig. 5. The results indicated that when wave height, period, and wind speed were high at offshore boundary, high WRS fields were recorded in the whole region. The wave fields recorded significant changes when they approached the shallow topography of the study beach. The main reason for these significant changes may be caused by the seabed topography complexity across the study area. The results of WRS in the coastal area pointed out that the wave height is complicatedly changed when the wave moves into the shallow water zones.

For WRS in the *xx*-direction (S_{xx}), the results pointed out that when the wave height at the offshore boundary is high the simulated values of S_{xx} are also high in the whole study domain (Fig. 5, *a*). When a wave moves into the shallower water zones, especially in the coastal zone, the results indicated that these are interlaced occurrences with large and small sizes of wave dispersion stress. The main cause of this interlaced occurrence is assessed due to complexity of the seabed topography. For WRS in the *xy*-direction (S_{xy}), the results indicated that the values of S_{xy} are small in the Northern part and large in the Southern part of the study area (Fig. 5, *b*). In addition, the results pointed out that the values of S_{xy} in the Northern part also decreased as the wave height increased. For instance, the simulated value of S_{xy} was 200 N/m when the wave height was 2.3 m; but when the value of S_{xy} was 35 N/m, the wave height was 0.9 m, while the values of S_{xy} in the Southern part increased corresponding to the increased wave height (e.g., the simulated values of S_{xy} varied from 100 to 300 N/m when the wave height was still 2.3 m, while the values of S_{xy} varied from 25 to 55 N/m when the wave height was 0.9 m).
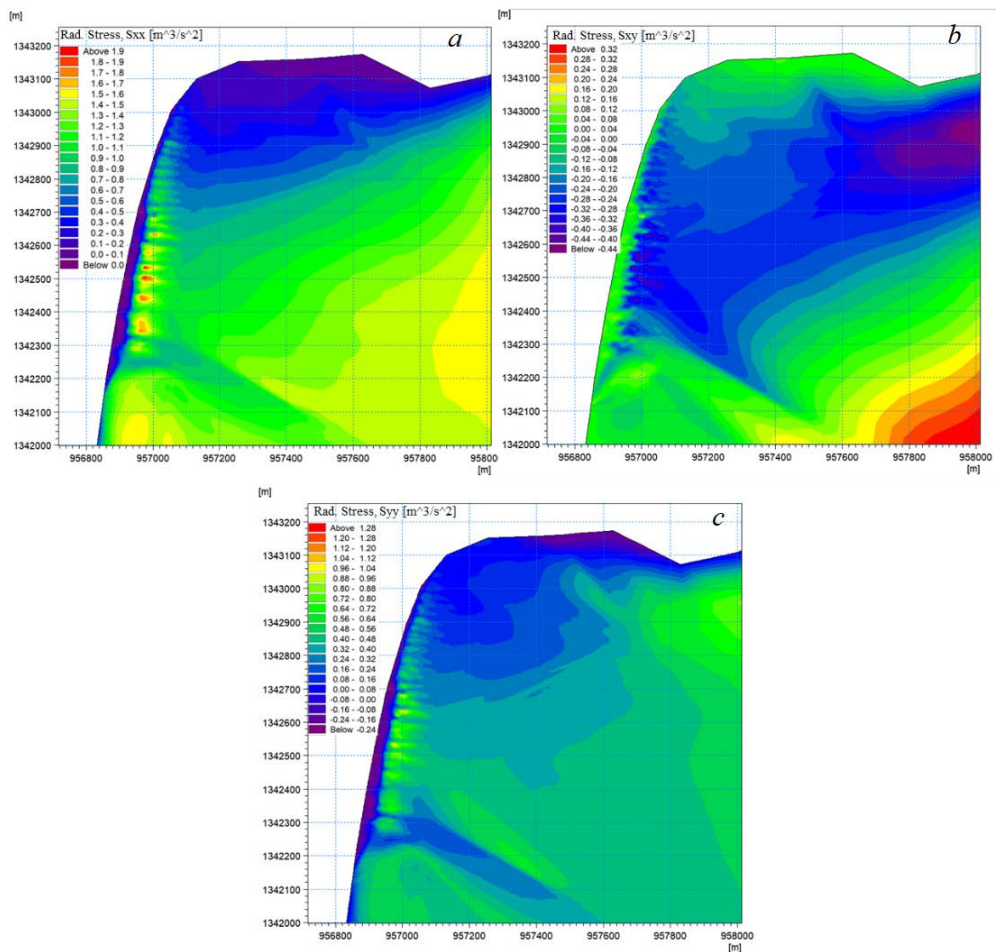

F i g. 5. Simulation of WRS components S_{xx} (*a*), S_{xy} (*b*) and S_{yy} (*c*) across the study area

The results also pointed out that the lowest values of S_{xy} were recorded in the Northern part of the study beach. The simulated results showed that the values of S_{xy} in the Northern part markedly decreased when the wave height from offshore increased.

For WRS in the yy-direction (S_{yy}), the results showed a similar tendency for S_{xx} (Fig. 5, c). The values of S_{yy} were small in the deep-water zone but the values of S_{yy} were large when entering the coastal area under the influence of shallower seabed terrain. The shallower seabed terrain led to a significant increase in the values of S_{yy} and it had alternating large and small values. Specifically, the higher wave height led to the greater values of S_{yy} (e.g., when the wave height was 2.3 m, the values of S_{yy} in the coastal zone varied from 350–550 N/m, when the wave height was 0.9 m, the values of S_{yy} varied from 70–110 N/m).

Simulation results of the current field. To facilitate the detection of the rip current occurrence as well as to analyze and compare the simulation results, the study area was divided into three sub-areas, which are shown in Fig. 6.
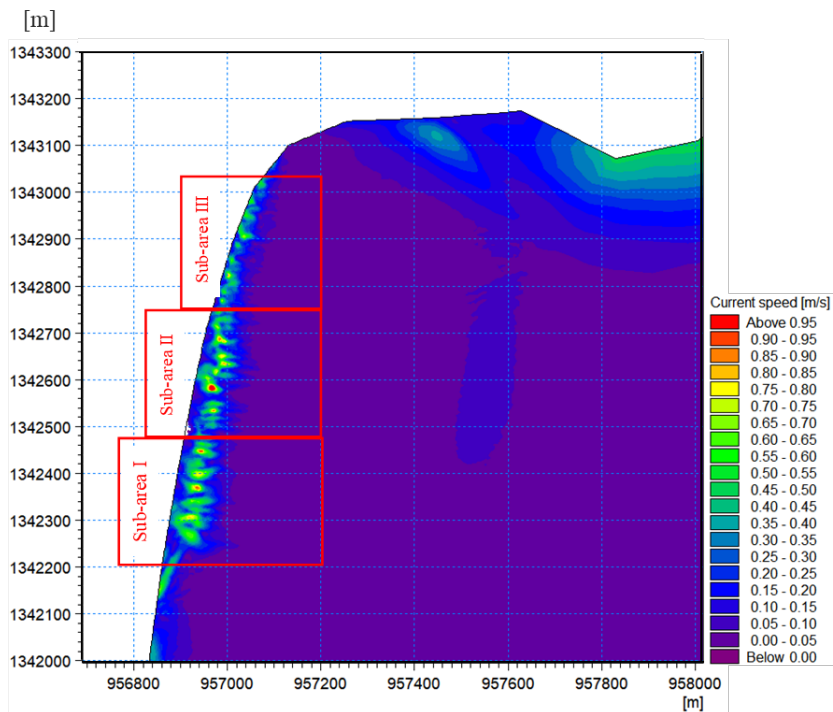
F i g. 6. Map of the study area with three sub-areas marked with red rectangles

The simulated results of the current fields across the study area are presented in Fig. 7. For sub-area I, when high wave heights appear, four rip currents can be clearly seen. All of them have a pretty similar structure and are created from two interference currents (Fig. 7, a). Especially, the second and the fourth rip currents from the North to the South of the sub-area I have a width up to 10 m and a current speed varying from 0.70 to 0.85 m/s.

For sub-area II, when high wave heights appear, five rip currents can be noted (Fig. 7, *b*). Among these five rip currents, the second and the third ones from the North to the South of sub-area II have a width of approximately 8 m and their current speed varies from 0.65 to 0.80 m/s. In general, with a high seaward current speed in the case of sub-areas I and II the rip currents can pull swimmers away from the shore when they are unlucky to swim into these areas. For sub-area III, the simulation indicated that when high wave heights appear, five rip currents can be clearly noted (Fig. 7, *c*). These rip currents have a pretty similar structure with narrow rip channel width (less than 4.0 m) and they mainly form vortex craters with current speed varying from 0.20 to 0.35 m/s.
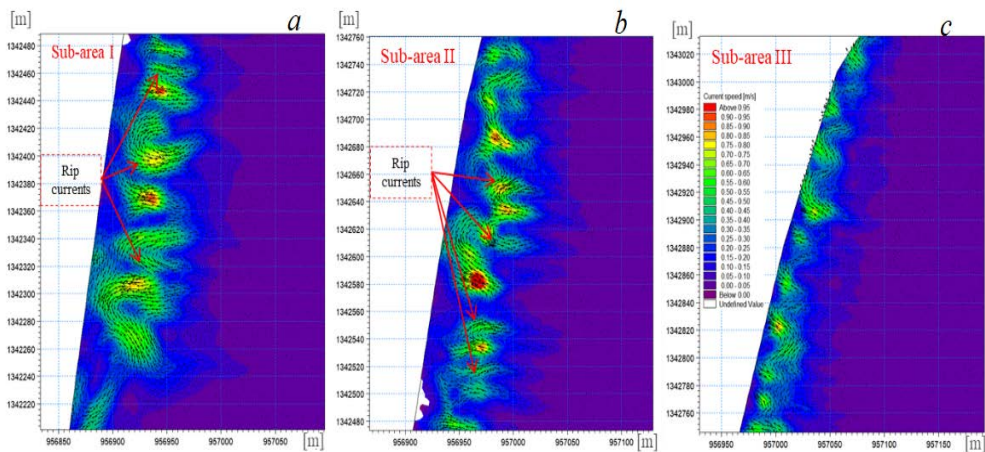
F i g. 7. Simulation of current fields across sub-area I (*a*), sub-area II (*b*), and sub-area III (*c*)

Conclusions

1. The study applied the MIKE21 Model for simulating the possibility of rip current generations across the Bai Dai Beach along Cam Ranh Bay of Khanh Hoa Province, Vietnam. Based on the findings the proposed model detected the rip current occurrence at different locations along the beach under study.

2. The results confirmed that when large wave heights and wind speeds occur, the rip currents with high current-speed prevail. In sub-areas I and II, rip currents with large rip-channel width and high current-speed up to 0.80 m/s were recorded, while in sub-area III the presence of vortices with low current-speed of approximately 0.20 m/s were recorded in the activity periods of the Northeast monsoon circulation.

3. Actual cases of drowning accidents related to rip currents recorded at simulated locations took place there.

REFERENCES

1.   Kim, H.D. and Kim, K.-H., 2021. Analysis of Rip Current Characteristics Using Dye Tracking Method. *Atmosphere*, 12(6), 719. doi:10.3390/atmos12060719

2.   Li, Z., 2016. Rip Current Hazards in South China Headland Beaches. *Ocean & Coastal Management*, 121, pp. 23-32. doi:10.1016/j.ocecoaman.2015.12.005

3.   Brander, R. and Scott, T., 2016. Science of the Rip Current Hazard. In: M. Tipton and A. Wooler, eds., 2016. *The Science of Beach Lifeguarding*. Boca Raton, Florida: CRC Press, pp. 67-86. doi:10.4324/9781315371641

4.   Castelle, B., Scott, T., Brander, R.W. and McCarroll, R.J., 2016. Rip Current Types, Circulation and Hazard. *Earth-Science Reviews*, 163, pp. 1-21. doi:10.1016/j.earscirev.2016.09.008

5.   Gensini, V.A. and Ashley, W.S., 2010. Reply to "Rip Current Misunderstandings". *Natural Hazards*, 55, pp. 163-165. doi:10.1007/s11069-010-9528-3

6.   MacMahan, J., Brown, J., Brown, J., Thornton, E., Reniers, A., Stanton, T., Henriquez, M., Gallagher, E., Morrison, J. [et al.], 2010. Mean Lagrangian Flow Behavior on an Open Coast Rip-Channeled Beach: A New Perspective. *Marine Geology*, 268(1-4), pp. 1-15. doi:10.1016/j.margeo.2009.09.011

7.   Austin, M.J., Scott, T.M., Russell, P.E. and Masselink, G., 2013. Rip Current Prediction: Development, Validation, and Evaluation of an Operational Tool. *Journal of Coastal Research*, 29(2), pp. 283-300. doi:10.2112/JCOASTRES-D-12-00093.1

8.   Leatherman, S.B. and Leatherman, S.P., 2017. Techniques for Detecting and Measuring Rip Currents. *International Journal of Earth Science and Geophysics*, 3(1), 014. doi:10.35840/2631-5033/1814

9.   McCarroll, R.J., Brander, R.W., MacMahan, J.H., Turner, I.L., Reniers, A.J.H.M., Brown, J.A. and Bradstreet, A., 2013. Assessing the Effectiveness of Rip Current Swimmer Escape Strategies, Shelly Beach, NSW, Australia. *Journal of Coastal Research,* 65(sp1), pp. 784-789. doi:10.2112/SI65-133.1

10.   Scott, T., Austin, M., Masselink, G. and Russell, P., 2016. Dynamics of Rip Currents Associated with Groynes – Field Measurements, Modelling and Implications for Beach Safety. *Coastal Engineering*, 107, pp. 53-69. doi:10.1016/j.coastaleng.2015.09.013

11.   Moulton, M., Dusek, G., Elgar, S. and Raubenheimer, B., 2017. Comparison of Rip Current Hazard Likelihood Forecasts with Observed Rip Current Speeds. *Weather and Forecasting*, 32(4), pp. 1659-1666. doi:10.1175/WAF-D-17-0076.1

12.   Winter, G., van Dongeren, A.R., de Schipper, M.A. and van Thiel de Vries, J.S.M., 2014. Rip Currents under Obliquely Incident Wind Waves and Tidal Longshore Currents. *Coastal Engineering*, 89, pp. 106-119. doi:10.1016/j.coastaleng.2014.04.001

13.   Brighton, B., Sherker, S., Brander, R., Thompson, M. and Bradstreet, A., 2013. Rip Current Related Drowning Deaths and Rescues in Australia 2004-2011. *Natural Hazards and Earth System Sciences*, 13(4), pp. 1069-1075. doi:10.5194/nhess-13-1069-2013

14.   Drozdzewski, D., Shaw, W., Dominey-Howes, D., Brander, R., Walton, T., Gero, A., Sherker, S., Goff, J. and Edwick, B., 2012. Surveying Rip Current Survivors: Preliminary Insights into the Experiences of Being Caught in Rip Currents. *Natural Hazards and Earth System Sciences*, 12(4), pp. 1201-1211. doi:10.5194/nhess-12-1201-2012

15.   Bonneton, P., Bruneau, N., Castelle, B. and Marche, F., 2010. Large-Scale Vorticity Generation Due to Dissipating Waves in the Surf Zone. *Discrete and Continuous Dynamical Systems - B*, 13(4), pp. 729-738. doi:10.3934/dcdsb.2010.13.729

16.   Wang, H., Zhu, S., Li, X., Zhang, W. and Nie, Y., 2018. Numerical Simulations of Rip Currents off Arc-Shaped Coastlines. *Acta Oceanologica Sinica*, 37, pp. 21-30. doi:10.1007/s13131-018-1197-1

17.   Bruneau, N., Bonneton, P., Castelle, B. and Pedreros, R., 2011. Modeling Rip Current Circulations and Vorticity in a High-Energy Mesotidal-Macrotidal Environment. *Journal of Geophysical Research: Oceans*, 116(C7), C07026. doi:10.1029/2010JC006693

18.   Hu, P., Li, Z., Zhu, D., Zeng, C., Liu, R., Cheng, Z. and Su, Q., 2022. Field Observation and Numerical Analysis of Rip Currents at Ten-Mile Beach, Hailing Island, China. *Estuarine, Coastal and Shelf Science*, 276, 108014. https://doi.org/10.1016/j.ecss.2022.108014

19.   Castelle, B., Michallet, H., Marieu, V., Leckler, F., Dubardier, B., Lambert, A., Berni, C., Bonneton, P., Barthélemy, E. and Bouchette, F., 2010. Laboratory Experiment on Rip Current

Circulations over a Moveable Bed: Drifter Measurements. *Journal of Geophysical Research: Oceans*, 115(C12), C12008. doi:10.1029/2010JC006343

20. Nguyex, X.L. and Dang, D.D., 2019. Assessing the Possibility of Appearing RIP Current at Quy Nhon Beach, Binh Dinh Province. *VNU Journal of Science: Earth and Environmental Sciences*, 35(4), pp. 34-47 doi:10.25073/2588-1094/vnuees.4416

21. Nguyen, K.P., Ngo, N.T. and Tran, T.H., 2012. [Researching to Calculate Rip Currents in Nha Trang Area]. *Journal of Water Resources Science and Technology*, 12, pp. 85-90 (in Vietnamese).

22. Le, D.M., 2005. Estimation of Wave Characteristics during Hurricane in Khanh Hoa Area. *Journal of Marine Science and Technology*, 2(5), pp. 1-17 (in Vietnamese).

23. Murray, T., Cartwright, N. and Tomlinson, R., 2013. Video-Imaging of Transient Rip Currents on the Gold Coast Open Beaches. *Journal of Coastal Research*, 65(sp2), pp. 1809-1814. doi:10.2112/SI65-306.1

About the authors:

Nam Thinh Ngo, Lecturer, VNU University of Science, Ho Chi Minh City University of Natural Resources and Environment (236B Le Van Sy Str., Ward 1, Tan Binh District, Ho Chi Minh City, Vietnam), Ph.D. (Sci.), **ORCID ID: 0000-0002-9939-4630**, nnthinh@hcmunre.edu.vn, thinhngnam@gmail.com

Thi Bay Nguyen, Associate Professor**,** Senior Lecturer, VNU Ho Chi Minh City, University of Technology (268 Ly Thuong Kiet Str., Ward 14, District 10, Ho Chi Minh City, Vietnam), **ORCID ID: 0000-0003-1815-8319**, ntbay@hcmut.edu.vn

Contribution of the co-authors:

Nam Thinh Ngo – discussed the original idea of the draft, designed the input data, performed the MIKE21-NSW Model simulation, analyzed the output data, wrote and edited the manuscript

Thi Bay Nguyen – discussed the original idea of the draft, wrote, reviewed and submitted the final version of the manuscript

The authors have read and approved the final manuscript.
The authors declare that they have no conflict of interest.